coatings

MDPI

Article

Effect of the Working Pressure and Oxygen Gas Flow Rate on the Fabrication of Single-Phase Ag_2O Thin Films

Jiyoon Choi [1,†], Jiha Seong [1,†], Sangbin Park [1], Hyungmin Kim [1], Sangmo Kim [2,*], Kyung Hwan Kim [1] and Jeongsoo Hong [1,*]

[1] Department of Electrical Engineering, Gachon University, 1342 Seongnamdaero, Seongnam 13120, Republic of Korea; wldbsl512@naver.com (J.C.); jiha0820@naver.com (J.S.); tkdrns7@naver.com (S.P.); kjf9252@gmail.com (H.K.); khkim@gachon.ac.kr (K.H.K.)
[2] Department of Intelligent Mechatronics Engineering, Sejong University, 209 Neungdong-ro, Gwangjin-gu, Seoul 05006, Republic of Korea
* Correspondence: sangmokim@sejong.ac.kr (S.K.); hongsj@gachon.ac.kr (J.H.)
† These authors contributed equally to this work.

Abstract: Ag_2O thin films have been applied in various devices, such as photodetectors, photocatalysts, and gas sensors, because of their excellent thermal stability, strong electrical properties, and stable structures. However, because various phases of silver oxide exist, the fabrication of single-phase Ag_2O thin films using a general deposition system is difficult. In this study, Ag_2O thin films were deposited on glass substrates at different working pressures and O_2 gas flow rates using a facing-target sputtering (FTS) system. After optimizing the working pressure and O_2 gas flow rate, the Ag_2O thin films were post-annealed at different temperatures ranging from 100 to 400 °C to improve their crystallographic properties. The X-ray diffraction patterns of the as-fabricated Ag_2O thin films indicated the presence of a single phase of Ag_2O, and the ultraviolet–visible (UV–vis) spectral analysis indicated transmittance of 65% in the visible light region. The optimum working pressure and O_2 gas flow rate were determined to be 4 mTorr and 3.4 sccm, respectively. Finally, the effect of the post-annealing temperature on the thin film was investigated; the Ag_2O peak had high intensity at 300 °C, suggesting this as the optimum post-annealing temperature.

Keywords: Ag_2O; working pressure; oxygen; post-annealing; FTS system

Citation: Choi, J.; Seong, J.; Park, S.; Kim, H.; Kim, S.; Kim, K.H.; Hong, J. Effect of the Working Pressure and Oxygen Gas Flow Rate on the Fabrication of Single-Phase Ag_2O Thin Films. *Coatings* **2023**, *13*, 1061. https://doi.org/10.3390/coatings13061061

Academic Editor: Alina Pruna

Received: 15 May 2023
Revised: 1 June 2023
Accepted: 3 June 2023
Published: 7 June 2023

1. Introduction

p–n junctions are widely employed in various applications, such as photodetectors and gas sensors [1,2]. Several materials are used for the construction of p–n junctions; among them, ZnO, β-Ga_2O_3, and MoS_2 have been used as n-type semiconductor materials, and silver oxide, copper oxide, and nickel oxide have been employed as p-type semiconductor materials for the manufacturing of p–n junction-based photodetectors [3,4]. In particular, Ag_xO_y (silver oxide) exists in different crystal forms, such as AgO, Ag_2O, Ag_3O_4, and Ag_2O_3, which result in different electrical, chemical, and optical properties [5–7]. Among them, Ag_2O exhibits a stable structure, excellent thermal stability, and photoreactivity [8,9]. Ag_2O has a cubic structure with six atoms per unit cell, and its lattice constant a = 0.47 nm. The optical band gap energies of Ag_2O thin films range across 1.2–3.4 eV depending on the fabrication method [10,11]. The thin films have been applied in many practical fields, such as gas sensors, photocatalysts, and photodetector manufacturing [12,13], owing to their excellent electrical properties and wide and strong light absorption in the visible light region [14]. However, fabricating single phase Ag_2O thin films using conventional deposition systems remains challenging [6].

Ag_2O thin films have been fabricated using various methods, including solution processing, sputtering, and e-beam evaporation [15–17]. Compared to other methods,

sputtering can deposit thin films at low temperatures with excellent deposition rates. Furthermore, the thicknesses and structures of thin films can be easily controlled by adjusting the sputtering conditions, such as the partial pressures of O_2 and Ar [18]. However, in a typical sputtering system, the substrate is located within the plasma area, which causes damage to the surfaces of the films owing to high-energy particle collisions, resulting in nonuniformity. In contrast, the structure of a facing-target sputtering (FTS) system comprises two targets facing each other, with the substrate being located outside the plasma area generated by the targets; this minimizes damage to the substrate and thin film due to the high-energy particles emitted during sputtering [19,20]. In addition, it enables the deposition of high-quality thin films because the high-speed accelerating particles moving between targets form a magnetic field with a high ionization rate [21,22].

In this study, Ag_2O thin films with excellent properties were fabricated by varying the working pressure and O_2 gas flow rate of an FTS system. The optimal working pressure and O_2 gas flow rate at which only Ag_2O existed without impurities were determined. The chemical compositions of the thin films fabricated under the optimal sputtering process conditions were confirmed from X-ray photoelectron spectroscopy (XPS) data. In addition, rapid thermal annealing (RTA) was conducted on the Ag_2O thin film fabricated under the optimal sputtering process conditions to improve the crystallographic properties and rearrange the atoms in the film [23,24]; changes in the properties caused by varying the annealing temperature over the range of 100–400 °C were investigated. Finally, the post-annealed Ag_2O thin films fabricated under the optimal sputtering process conditions were evaluated using X-ray diffraction (XRD) and UV–vis spectroscopy.

2. Experimental Section

2.1. Fabrication

Each Ag_2O thin film was deposited on a soda–lime glass substrate (75 mm × 25 mm; thickness: 1 mm; Marienfeld, Lauda-Königshofen, Germany) with 4-inch Ag targets (99.99%; RND Korea, Gwangmyeong-si, Republic of Korea) using an FTS system, as shown in Figure 1. The glass was ultrasonically cleaned for 10 min with isopropanol (C_3H_8O; 99.5%, extra pure; Daejung Chemicals & Metals Co., Ltd., 186 Seohaean-ro, Siheung-si, Republic of Korea) and acetone (C_2H_6O; 99.5%, extra pure; Daejung Chemicals & Metals Co., Ltd., 186 Seohaean-ro, Siheung-si, Republic of Korea), following which it was rinsed with deionized water. N_2 gas was blown to remove watermarks, and the samples were finally dried in an oven for 15 min. Table 1 lists the sputtering conditions for the Ag_2O thin films. For sputtering, 4-inch Ag targets (99.99%; RND Korea, Gwangmyeong-si, Republic of Korea) were used, and samples were deposited at different working pressures and O_2 gas flow rates. A post-annealing process was conducted to investigate the effect of the annealing temperature on the properties of the Ag_2O thin films using rapid thermal annealing (RTA). The post-annealing temperature was varied from 100 to 400 °C at intervals of 100 °C.

Table 1. Sputtering conditions for Ag_2O thin films.

Parameters	Conditions
Thickness	150 nm
Targets	Ag (99.99%), 4″
Substrate	Soda–lime glass
Input power	50 W
Working pressure	1, 2, 3, and 4 mTorr
Gas flow rate	O_2: 2.5, 3.4, and 5 sccm; Ar: 10 sccm

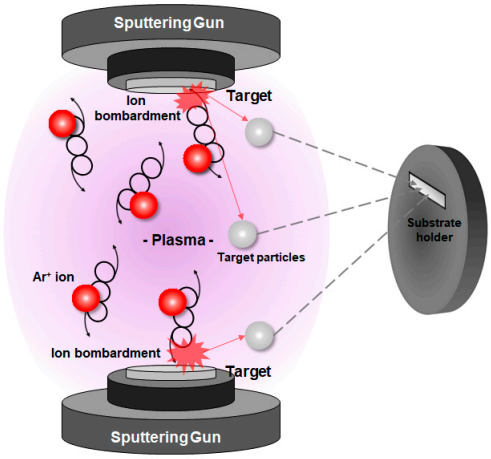

Figure 1. Schematic of the Facing Targets Sputtering (FTS) system.

2.2. Evaluation of Samples

To optimize the oxygen flow rate and working pressure conditions, Ag_2O thin films with a thickness of 150 nm were deposited on glass substrates, and their properties were analyzed with respect to changes in the O_2 gas flow rate and working pressure.

The electrical, structural, and optical properties of the fabricated Ag_2O films were analyzed. The crystallographic properties of the thin films were evaluated using XRD (Smartlab, Rigaku, Tokyo, Japan) at the Smart Materials Research Center for IoT, Gachon University. Scanning electron microscopy (SEM; SU8600, Hitachi, Tokyo, Japan) was used to observe the surface morphology. XPS (K-alpha+, Thermo Fisher Scientific, Waltham, MA, USA) was used to investigate the composition ratio and binding energy of Ag. The thicknesses of the as-fabricated Ag_2O films were measured using an Alpha-Step profilometer (Alpha-Step-500 Profiler, KLA-Tencor, Milpitas, CA, USA). The optical properties of the samples, such as transmittance and optical bandgap energy, were evaluated using a UV–vis spectrometer (Lambda 750 UV–vis–NIR, Perkin Elmer, Waltham, MA, USA).

3. Results and Discussion

3.1. Evaluation of Ag_2O Thin Films

Figure 2A shows the XRD patterns of as-deposited Ag_2O thin films fabricated at a constant working pressure of 4 mTorr and varied O_2 gas flow rates of 2.5–5.0 sccm. In the case of 2.5 sccm, a Ag peak appeared at $2\theta = 64.7^\circ$ corresponding to the (220) plane (JCPDS File No. 04-0783). In addition, the peaks of the (100) and (002) planes of Ag_2O (ICDD card 01-072-2108) were observed, representing a mixed phase of Ag and Ag_2O. For the film deposited at 3.4 sccm, Ag_2O peaks were observed at $2\theta = 33.6^\circ$ and 55.7° without the presence of other impurity peaks, and the intensity of the Ag_2O peak at $2\theta = 33.6^\circ$ increased with the increasing O_2 gas flow rate. However, for the film deposited at 5.0 sccm, AgO peaks appeared at $2\theta = 32.3^\circ$ (JCPDS File No. 84-1547), and no Ag_2O peaks were observed. Therefore, as the O_2 gas flow rate increased, a phase change occurred. This is because the increase in the O_2 gas flow rate resulted in the reaction of the sputtered Ag metal atoms in the chamber with the O atoms, forming silver oxides in the presence of plasma [9]. Thereafter, based on the XRD data, the crystallite sizes of the samples were calculated using the Debye–Scherrer equation [25]. The Debye–Scherrer equation is as follows:

$$\tau = \frac{K\lambda}{\beta cos\theta} \quad (1)$$

where β is the full width at half-maximum (FWHM); τ is the crystallite size; θ is the Bragg angle; K is the Scherrer constant (0.9); and λ is the X-ray wavelength.

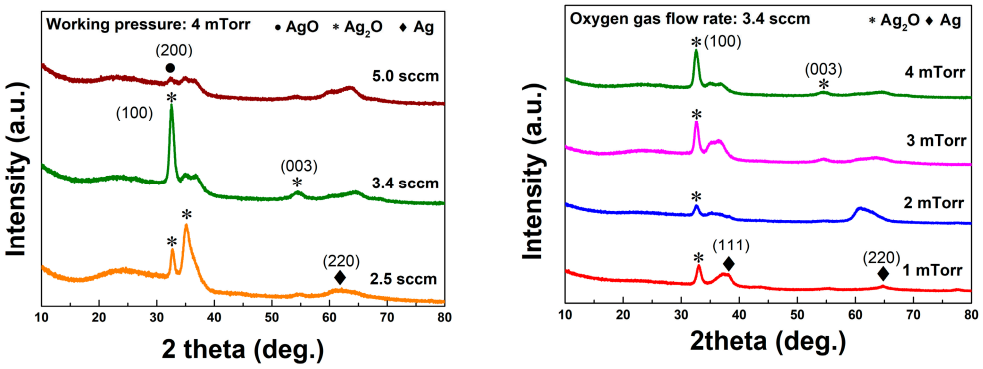

Figure 2. (**A**) XRD patterns of thin films deposited at different O_2 gas flow rates. (●: AgO; ◆: Ag; ∗: Ag_2O). (**B**) XRD patterns of thin films deposited at different working pressures (●: AgO; ◆: Ag; ∗: Ag_2O).

Table 2 lists the calculated crystallographic parameters of the Ag_2O thin films deposited at different O_2 gas flow rates. When the O_2 gas flow rate was increased, the lattice constant also increased because of the presence of interstitial oxygen, which expanded the lattice [26].

Table 2. Calculated lattice constants and crystallite sizes of Ag_2O films deposited at various O_2 gas flow rates.

O_2 Gas Flow Rate (sccm)	Lattice Constant (Å)	Crystallite Size (nm)
2.5	4.65	8.63
3.4	4.67	11.25
5.0	4.77	15.68

Figure 2B shows the XRD patterns of the as-deposited Ag_2O thin films obtained by varying the working pressure from 1 to 4 mTorr. The thin films were fabricated at the same O_2 gas flow rate of 3.4 sccm, and the working pressures were changed from 1 to 2, 3, and 4 mTorr. At 1 mTorr, Ag peaks appeared at 2θ = 38.2° and 64.7°, corresponding to the (111) and (220) planes, respectively. Furthermore, the (100) peak of Ag_2O was observed, indicating a mixed phase of Ag and Ag_2O. At 2 and 3 mTorr, the intensity of the Ag_2O peak was lower than that at 4 mTorr. Meanwhile, the intensity of the peaks related to the (100) and (003) planes of Ag_2O, which represented the intensity of the Ag_2O peak, increased the most in the film deposited at 4 mTorr. Therefore, a working pressure of 4 mTorr and an O_2 gas flow rate of 3.4 sccm were determined to be the optimal conditions for the fabrication of single-phase Ag_2O thin films. Table 3 lists the calculated crystallographic parameters of Ag_2O thin films deposited at different working pressures; the films exhibited no significant changes.

Table 3. Calculated lattice constants and crystallite sizes of Ag_2O films deposited at various working pressures.

Working Pressure (mTorr)	Lattice Constant (Å)	Crystallite Size (nm)
1	4.71	12.77
2	4.66	12.13
3	4.66	12.49
4	4.67	11.25

Figure 3A–D compare the SEM images of Ag_2O thin films deposited at working pressures of 1, 2, 3, and 4 mTorr, respectively. As shown in Figure 3B,C, the surfaces of the

thin films deposited at 2 and 3 mTorr were not homogeneous, and the grains were unclear. As expected, the observance of the broad peaks of amorphous AgO_x at 2 and 3 mTorr in the XRD patterns was in agreement with the results of the SEM images.

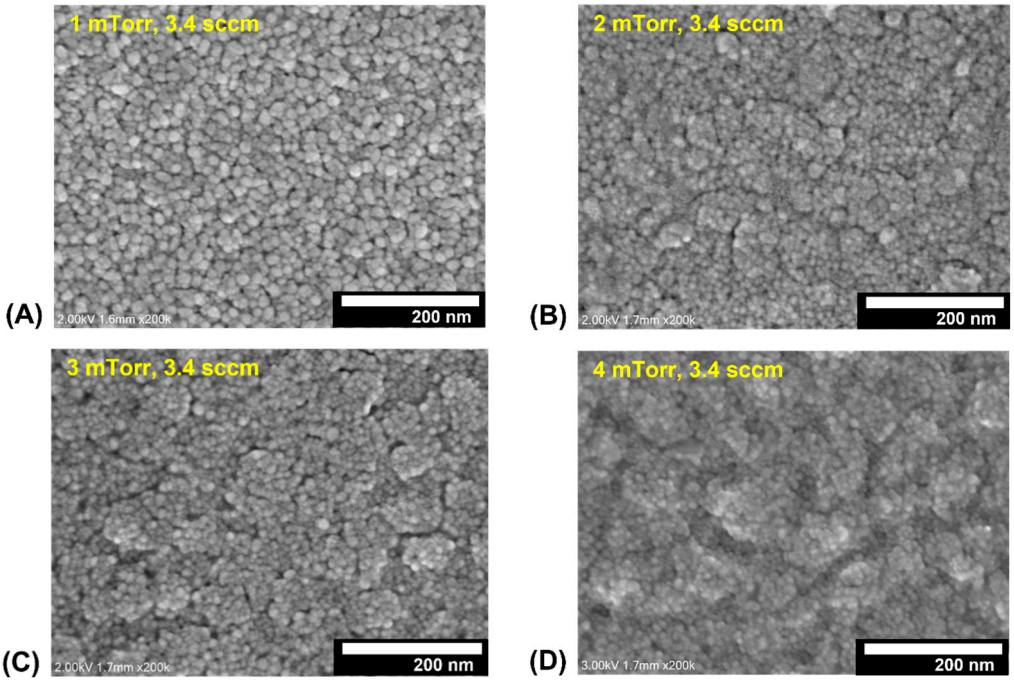

Figure 3. SEM surface morphology images of Ag_2O thin films deposited at a constant O_2 gas flow rate of 3.4 sccm and different working pressures of (**A**) 1, (**B**) 2, (**C**) 3, and (**D**) 4 mTorr.

Figure 4 shows the UV–vis spectra of the Ag_2O thin films deposited at different working pressures and O_2 gas flow rates. Figure 4A shows the UV–vis spectra of the thin films deposited at working pressures of 1, 2, 3, and 4 mTorr and an O_2 gas flow rate of 3.4 sccm. A change in the UV–vis spectra was observed when the thin film changed from mixed-phase to single-phase Ag_2O. Similar UV–vis spectra were observed for the single-phase Ag_2O obtained at working pressures of 3 and 4 mTorr. Furthermore, UV–vis spectral analysis could explain the transition from a mixed phase to a single phase. As shown in Figure 4A, the samples deposited at working pressures of 1 and 2 mTorr exhibited low transmittance. This is because the patterns of the two samples exhibited mixed peaks of Ag and Ag_2O, based on the XRD results. However, the thin films deposited at working pressures of 3 and 4 mTorr had high transmittance, indicating that at working pressures >3 mTorr, single-phase Ag_2O thin films were formed [27]. In this study, the samples deposited at a working pressure of 4 mTorr exhibited the clearest XRD peak and the highest transparency at a wavelength of approximately 790 nm. However, the spectra of samples deposited at 1, 2, and 3 mTorr, in which a mixed phase of Ag and Ag_2O was formed, exhibited the highest transmittance at wavelengths over 800 nm. Figure 4B shows the UV–vis spectra of Ag_2O thin films deposited at a working pressure of 4 mTorr and O_2 gas flow rates of 2.5, 3.4, and 5 sccm. The transmittance of the films decreased when the O_2 gas flow rate was increased from 3.4 to 5 sccm. Based on the XRD analysis, at a working pressure of 4 mTorr, AgO appeared when the O_2 gas flow rate was increased from 3.4 to 5 sccm. Consequently, the decrease in transmittance was due to light scattering, which occurs when two or more phases are present. Figure 4C,D show the optical bandgap energies of the as-deposited and post-annealed Ag_2O thin films calculated using the Tauc plot equation. Based on the optimal conditions determined from the XRD and UV–vis spectral analysis results, the optical bandgap energy of the Ag_2O thin film deposited at a working pressure of 4 mTorr and an O_2 gas flow rate of 3.4 sccm was calculated. The optical band gap energy was calculated using the Tauc plot equation [28]. The Tauc plot was used

to determine the band gap using the optical absorbance data plotted appropriately with respect to energy [29].

$$\alpha h\upsilon = \beta(h\upsilon - E_g)^n \quad (2)$$

where h is Planck's constant; α is the absorption coefficient; υ is the frequency of the photon; E_g is the band gap; β is the slope of the Tauc plot in the linear region; and n is the power coefficient, which depends on the transition type. As the Ag_2O film had a direct allowed transition, $n = 1/2$ was used in the above equation [30,31]. The optical bandgap energy of the Ag_2O thin film deposited at a working pressure of 4 mTorr and an O_2 gas flow rate of 3.4 sccm was calculated to be 3.16 eV.

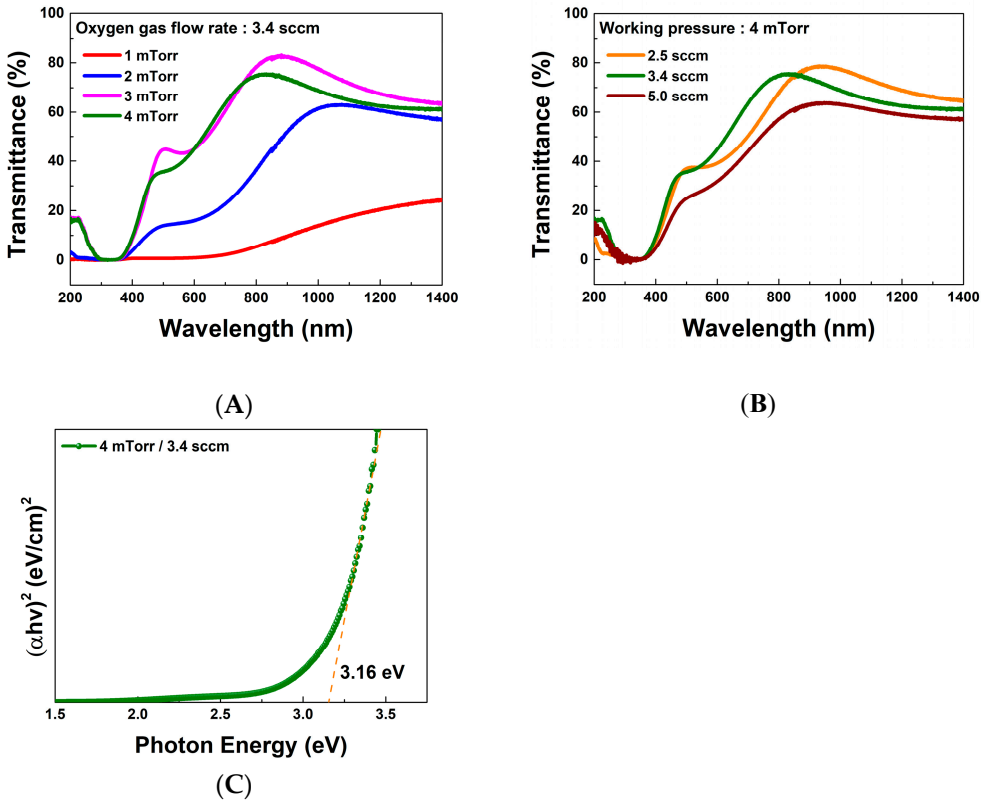

Figure 4. UV–vis spectra of Ag_2O thin films deposited at (**A**) constant O_2 gas flow rate and different working pressures and (**B**) constant working pressure and different O_2 gas flow rates. (**C**) Optical band gap energy of the as-deposited thin film deposited under the optimal conditions.

Table 4 lists the ratios of Ag and O in the Ag_2O thin films. The O to Ag ratio was also calculated. Comparing the samples deposited at the same O_2 gas flow rate of 3.4 sccm, as the working pressure increased, the amount of O also increased. Similarly, when the working pressure was constant and the O_2 gas flow rate was varied from 2.5 to 3.4 and 5.0 sccm, the amount of O increased. Figure 5A,B show the XPS spectra of Ag and O in the Ag_2O thin films deposited at an O_2 gas flow rate of 3.4 sccm. Although the amount of O_2 used for sputtering was the same, the O 1s peak intensity in the XPS spectrum increased with increasing working pressure. This phenomenon confirms that a high working pressure facilitates an efficient reaction of O_2 with Ag. As shown in Figure 5A, the samples deposited at 3 and 4 mTorr had higher Ag3d peaks than the samples deposited at 1 and 2 mTorr. The difference in the stoichiometry of Ag oxides was the reason for this. As we observed from the XRD result, at the O_2 gas flow rate of 3.4 sccm, the mixed phase of Ag and Ag_2O at the working pressure of 1 and 2 mTorr changed into the single-phase Ag_2O at the working pressure of 3 and 4 mTorr. This concludes that the difference in the stoichiometry of the Ag oxides caused the change in the peak [32]. Moreover, the O 1s peak shifted slightly to the right, to a higher binding energy, as shown in Figure 5B. This is because the samples

were exposed to air before XPS analysis and contaminated [33]. Figure 5C,D show the XPS spectra of Ag and O, respectively, for the Ag_2O thin films deposited at a working pressure of 4 mTorr.

Table 4. Ag and O content ratios of Ag_2O thin films.

Sample Identifier	Ag 3d%	O 1s%	Oxygen Versus Silver
1 mTorr, 3.4 sccm	28.30	16.03	1.77
2 mTorr, 3.4 sccm	25.05	16.41	1.53
3 mTorr, 3.4 sccm	33.67	22.08	1.52
4 mTorr, 2.5 sccm	31.92	20.29	1.57
4 mTorr, 3.4 sccm	33.55	23.80	1.50
4 mTorr, 5.0 sccm	26.98	19.30	1.40

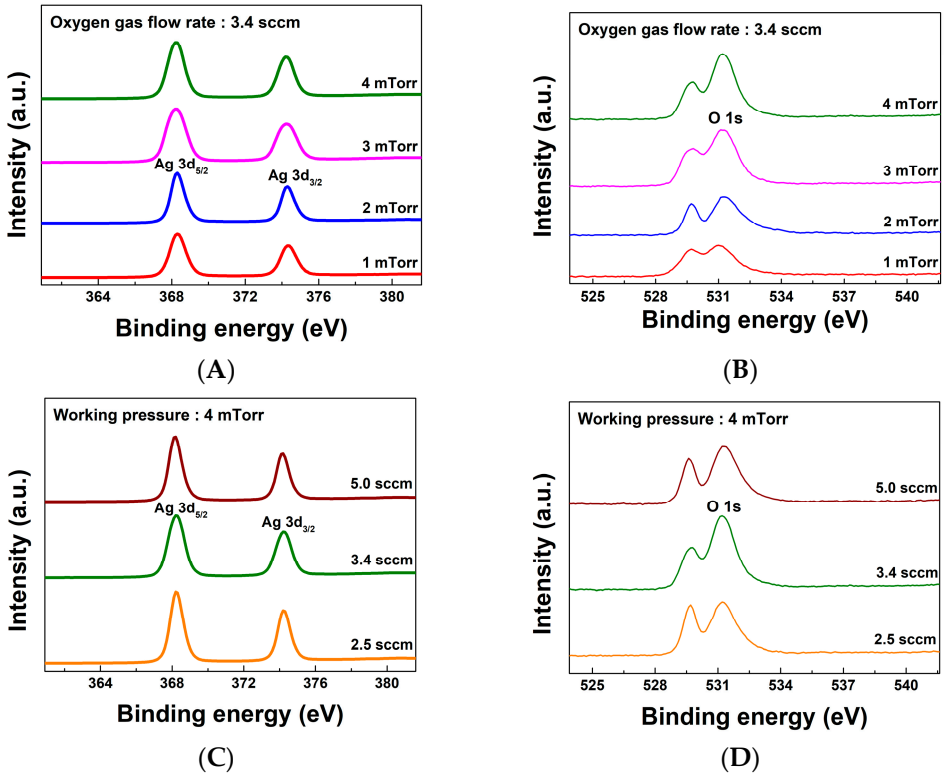

Figure 5. XPS spectra of Ag_2O thin films. (**A**) XPS spectra of Ag in the Ag_2O thin films deposited at 3.4 sccm. (**B**) XPS spectra of O_2 in the Ag_2O thin films deposited at 3.4 sccm. (**C**) XPS spectra of Ag in the Ag_2O thin films deposited at 4 mTorr. (**D**) XPS spectra of O_2 in the Ag_2O thin films deposited at 4 mTorr.

3.2. Evaluation of Ag_2O Thin Films Post-Annealed at RT to 400 °C

The effect of post-annealing on the Ag_2O thin films was also evaluated. An appropriate post-annealing temperature improves the quality of thin films by reducing the internal defects [34]. As the crystallographic properties of the deposited Ag_2O thin films were affected by the post-annealing temperature, heat treatment using RTA was performed to investigate the variation in the structural properties of Ag_2O.

Figure 6 shows the XRD patterns of Ag_2O thin films post-annealed at room temperature (RT) and at 100, 200, 300, and 400 °C. The films were deposited at a working pressure of 4 mTorr and an O_2 gas flow rate of 3.4 sccm. As the post-annealing temperature was increased from 100 to 300 °C, the Ag_2O peak intensity also increased. The Ag_2O peak intensity at $2\theta = 33.6°$ increased the most at 300 °C, indicating that the crystallite size increased with the increasing annealing temperature (RT: 11.31 nm, 100 °C: 12.66 nm, 200 °C: 16.02 nm, 300 °C: 20.45 nm, and 400 °C: 19.16 nm). These results indicate that the crys-

tallinity of the thin films improved with an increase in the post-annealing temperature [35]. However, as the post-annealing temperature was increased from 300 to 400 °C, the intensity of the Ag_2O peak at $2\theta = 33.6°$ slightly decreased. Moreover, at the annealing temperature of 400 °C, a Ag peak was observed at $2\theta = 44.5°$, which corresponded to the (200) plane. This indicated that the Ag_2O single phase was changed to a mixed phase of Ag and Ag_2O after heat treatment at 400 °C. This is because most of the oxygen atoms were diffused to the surface of the thin film; it was adsorbed in the form of oxygen molecules or escaped from the surface [36].

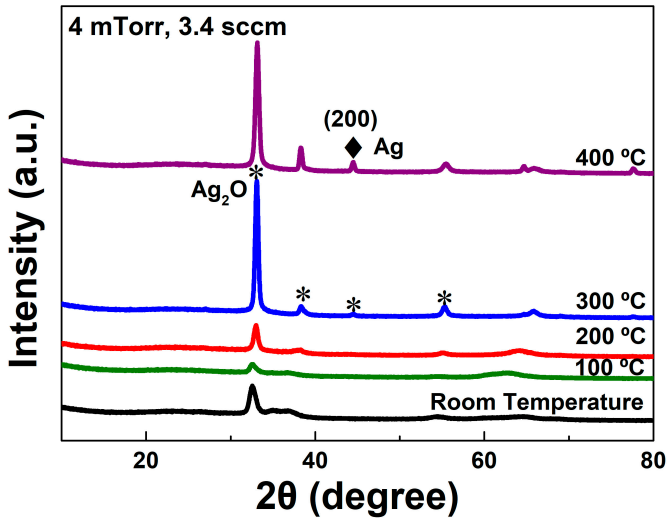

Figure 6. XRD patterns of Ag_2O thin films post-annealed at different temperatures in the range of room temperature (R.T.)–400 °C (◆: Ag; ∗: Ag_2O).

A Ag_2O thin film was deposited under the optimal conditions of a working pressure of 4 mTorr and an O_2 gas flow rate of 3.4 sccm and then post-annealed at a temperature of 300 °C. Figure 7A shows the UV–vis spectra and optical bandgap energy of the film deposited at the optimal working pressure and oxygen flow rate and post-annealed at 300 °C. The Ag_2O thin film post-annealed at 300 °C showed transmittance and optical band gap energy values similar to those of the as-deposited Ag_2O thin film.

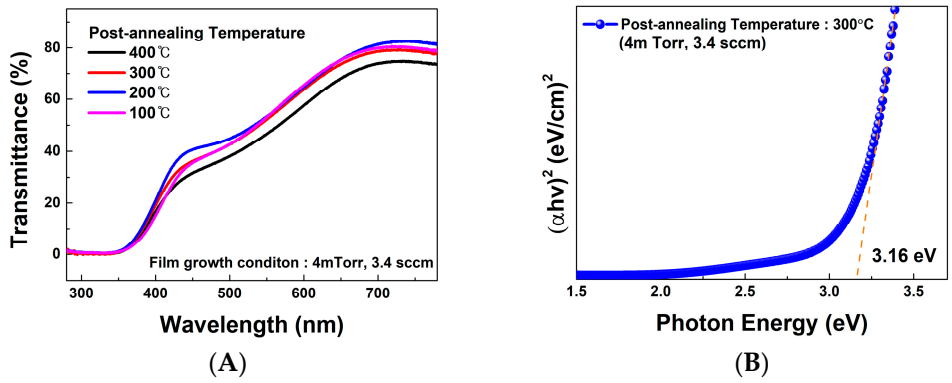

Figure 7. UV–vis spectra and optical band gap energy of the Ag_2O thin film. (**A**) UV–vis spectra of the thin film post-annealed at different temperatures. (**B**) Optical band gap energy of the thin film post-annealed at 300 °C.

4. Conclusions

Ag_2O thin films were deposited using an FTS system. The optimal conditions for the fabrication of the single-phase Ag_2O thin films were determined using various measurements. In the XRD pattern of the thin film deposited at a working pressure of 4 mTorr and

an oxygen flow rate of 3.4 sccm, only the Ag_2O peak appeared, and peaks corresponding to impurities were not observed. In addition, transmittance of 65% was observed in the visible light region in the UV–vis spectra. Furthermore, the influence of the post-annealing temperature on the thin films was investigated by varying the temperature from 100 to 400 °C and using XRD and crystallinity data. The Ag_2O peak intensity increased the most when the post-annealing temperature was increased from 100 to 300 °C, and the crystallite size also increased at 300 °C. XPS analysis confirmed that a higher working pressure caused a greater amount of O_2 to react with Ag. Future study of electric devices using p–n junctions with a single-phase Ag_2O thin film will be conducted.

Author Contributions: Writing—original draft preparation, J.C. and J.S.; Investigation and Analysis, S.P. and H.K.; Review and Editing, S.K.; Review and analysis, K.H.K.; Editing and Supervision, J.H. All authors have read and agreed to the published version of the manuscript.

Funding: This research was supported by a Korea Institute for Advancement of Technology (KIAT) grant funded by the Korea Government (MOTIE) (P0012451, The Competency Development Program for Industry Specialist) and the Basic Science Research Capacity Enhancement Project through a Korea Basic Science Institute (National Research Facilities and Equipment Center) grant funded by the Ministry of Education (2019R1A6C1010016).

Institutional Review Board Statement: Not applicable.

Informed Consent Statement: Not applicable.

Data Availability Statement: Not applicable.

Conflicts of Interest: The authors declare no conflict of interest.

References

1. Park, T.; Park, S.; Min, J.; Jung, Y.; Kyoung, S.; Kang, T.; Kim, K.; Rim, Y.; Hong, J. Temperature-Dependent Self-Powered Solar-Blind Photodetector Based on Ag_2O/β-Ga_2O_3 Heterojunction. *Nanomaterials* **2022**, *12*, 2983. [CrossRef] [PubMed]
2. Liang, Y.; Hsu, Y. Design of thin-film configuration of SnO_2–Ag_2O composites for NO_2 gas-sensing applications. *Nanotechnol. Rev.* **2022**, *11*, 1842–1853. [CrossRef]
3. Kumar, K.; Yadav, R.; Devi, S.; Singh, P.; Husale, S.; Tyagi, S.; Kaur, D. Effective ways to enhance the performance of n-MoS_2/p-CuO heterojunction based self-powered photodetectors. *Sol. Energy Mater. Sol. Cells* **2023**, *255*, 112285. [CrossRef]
4. Debnath, R.; Xie, T.; Wen, B.; Li, W.; Ha, J.Y.; Sullivan, N.F.; Nguyen, N.V.; Motayed, A. A solution-processed high-efficiency p-NiO/n-ZnO heterojunction photodetector. *Rsc Adv.* **2015**, *5*, 14646–14652. [CrossRef]
5. Nwanya, A.C.; Ugwuoke, P.E.; Ezekoye, B.A.; Osuji, R.U.; Ezema, F.I. Structural and optical properties of chemical bath deposited silver oxide thin films: Role of deposition time. *Adv. Mater. Sci. Eng.* **2013**, *2013*, 450820. [CrossRef]
6. Korkmaz, N.; Karadağ, A. Microwave assisted green synthesis of Ag, Ag_2O, and Ag_2O_3 nanoparticles. *J. Turk. Chem. Soc. Sect. A Chem.* **2021**, *8*, 585–592. [CrossRef]
7. Laskri, A.; Drici, A.; Boulouma, A.; Amara, A.; Bernede, J.C. Investigation of microstructural and optical properties of Ag_3O_4 thin films sprayed onto glass substrate. *J. Nano Res.* **2019**, *58*, 90–101. [CrossRef]
8. Salim, E.T.; Awayiz, M.T.; Mahdi, R.O. Tea concentration effect on the optical, structural, and surface roughness of Ag_2O thin films. *Dig. J. Nanomater. Biostruct.* **2019**, *14*, 1151–1159.
9. Pierson, J.F.; Rousselot, C. Stability of reactively sputtered silver oxide films. *Surf. Coat. Technol.* **2005**, *200*, 276–279. [CrossRef]
10. Fortin, E.; Weichman, F.L. photoconductivity in Ag_2O. *Phys. Status Solidi (B)* **1964**, *5*, 515–519. [CrossRef]
11. Barik, U.K.; Srinivasan, S.; Nagendra, C.L.; Subrahmanyam, A. Electrical and optical properties of reactive DC magnetron sputtered silver oxide thin films: Role of oxygen. *Thin Solid Film.* **2003**, *429*, 129–134. [CrossRef]
12. Jamal, R.K.; Mutlak, F.A.; Ibrahim, F.T.; Nayef, U.M. Synthesis of Ag_2O films by pulsed laser deposited on porous silicon as gas sensor application. *Optik* **2020**, *218*, 164971. [CrossRef]
13. Wang, X.; Li, S.; Yu, H.; Yu, J.; Liu, S. Ag_2O as a new visible-light photocatalyst: Self-stability and high photocatalytic activity. *Chem. A Eur. J.* **2011**, *17*, 7777–7780. [CrossRef]
14. Fang, F.; Li, Q.; Shang, J.K. Enhanced visible-light absorption from Ag_2O nanoparticles in nitrogen-doped TiO_2 thin films. *Surf. Coat. Technol.* **2011**, *205*, 2919–2923. [CrossRef]
15. Satyanarayana, N.; Xie, X.; Rambabu, B. Sol–gel synthesis and characterization of the Ag_2O–SiO_2 system. *Mater. Sci. Eng. B* **2000**, *72*, 7–12. [CrossRef]
16. Narayana Reddy, P.; Sreedhar, A.; Hari Prasad Reddy, M.; Uthanna, S.; Pierson, J.F. The effect of oxygen partial pressure on physical properties of nano-crystalline silver oxide thin films deposited by RF magnetron sputtering. *Cryst. Res. Technol.* **2011**, *46*, 961–966. [CrossRef]

17. Saroja, G.; Vasu, V.; Nagarani, N. Optical Studies of Ag_2O thin film prepared by electron beam evaporation method. *Open J. Met.* **2013**, *3*, 57–63. [CrossRef]
18. Entezar Mehdi, H.; Hantehzadeh, M.R.; Valedbagi, S. Physical properties of silver oxide thin film prepared by DC magnetron sputtering: Effect of oxygen partial pressure during growth. *J. Fusion Energy* **2013**, *32*, 28–33. [CrossRef]
19. Lee, M.; Park, Y.; Kim, K.; Hong, J. Influence of sputtering conditions on the properties of aluminum-doped zinc oxide thin film fabricated using a facing target sputtering system. *Thin Solid Film.* **2020**, *703*, 137980. [CrossRef]
20. Hong, J.; Jang, K.; Park, Y.; Choi, H.; Kim, K. Preparation of ZnO based thin films for OLED anode by facing targets sputtering system. *Mol. Cryst. Liq. Cryst.* **2011**, *538*, 103–111. [CrossRef]
21. Park, S.; Yoon, Y.; Lee, S.; Park, T.; Kim, K.; Hong, J. Thermoinduced and Photoinduced Sustainable Hydrophilic Surface of Sputtered-TiO_2 Thin Film. *Coatings* **2021**, *11*, 1360. [CrossRef]
22. Hong, J.; Matsushita, N.; Kim, K.H. Investigation of the effect of oxygen gas on properties of GAZO thin films fabricated by facing targets sputtering system. *Semicond. Sci. Technol.* **2014**, *29*, 075007. [CrossRef]
23. Araújo, A.; Mendes, M.J.; Mateus, T.; Vicente, A.; Nunes, D.; Calmeiro, T.; Fortunato, E.; Aguas, H.; Martins, R. Influence of the substrate on the morphology of self-assembled silver nanoparticles by rapid thermal annealing. *J. Phys. Chem. C* **2016**, *120*, 18235–18242. [CrossRef]
24. Mirzaeian, M.; Ogwu, A.A.; Jirandehi, H.F.; Aidarova, S.; Ospanova, Z.; Tsendzughul, N. Surface characteristics of silver oxide thin film electrodes for supercapacitor applications. *Colloids Surf. A Physicochem. Eng. Asp.* **2017**, *519*, 223–230. [CrossRef]
25. Fatimah, S.; Ragadhita, R.; Al Husaeni, D.F.; Nandiyanto, A.B.D. How to calculate crystallite size from x-ray diffraction (XRD) using Scherrer method. *ASEAN J. Sci. Eng.* **2022**, *2*, 65–76. [CrossRef]
26. Yang, J.L.; Lai, Y.S.; Chen, J.S. Effect of heat treatment on the properties of non-stoichiometric p-type nickel oxide films deposited by reactive sputtering. *Thin Solid Film.* **2005**, *488*, 242–246. [CrossRef]
27. Hanaor, D.A.H.; Triani, G.; Sorrell, C.C. Morphology and photocatalytic activity of highly oriented mixed phase titanium dioxide thin films. *Surf. Coat. Technol.* **2011**, *205*, 3658–3664. [CrossRef]
28. Hong, J.; Katsumata, K.-i.; Matsushita, N. Fabrication of Al-Doped ZnO Film with High Conductivity Induced by Photocatalytic Activity. *J. Electron. Mater.* **2016**, *45*, 4875–4880. [CrossRef]
29. Coulter, J.B.; Birnie, D.P. Assessing Tauc Plot Slope Quantification: ZnO Thin Films as a Model System. *Phys. Status Solidi Basic Res.* **2018**, *255*, 1700393. [CrossRef]
30. Park, S.; Park, T.; Park, J.H.; Min, J.Y.; Jung, Y.; Kyoung, S.; Kang, T.Y.; Kim, K.H.; Rim, Y.S.; Hong, J. Ag_2O/β-Ga_2O_3 Heterojunction-Based Self-Powered Solar Blind Photodetector with High Responsivity and Stability. *ACS Appl. Mater. Interfaces* **2022**, *14*, 25648–25658. [CrossRef]
31. Tsendzughul, N.T.; Ogwu, A.A. Physicochemical Aspects of the Mechanisms of Rapid Antimicrobial Contact-Killing by Sputtered Silver Oxide Thin Films under Visible Light. *ACS Omega* **2019**, *4*, 16847–16859.
32. Firet, N.J.; Blommaert, M.A.; Burdyny, T.; Venugopal, A.; Bohra, D.; Longo, A.; Smith, W.A. Operando EXAFS study reveals presence of oxygen in oxide-derived silver catalysts for electrochemical CO_2 reduction. *J. Mater. Chem. A* **2019**, *7*, 2597–2607. [CrossRef]
33. Pinto, G.; Dante, S.; Rotondi, S.M.C.; Canepa, P.; Cavalleri, O.; Canepa, M. Spectroscopic Ellipsometry Investigation of a Sensing Functional Interface: DNA SAMs Hybridization. *Adv. Mater. Interfaces* **2022**, *9*, 2200364. [CrossRef]
34. Gao, C.; Huang, J.; Li, H.; Sun, K.; Lai, Y.; Jia, M.; Jiang, L.; Liu, F. Fabrication of Sb_2S_3 thin films by sputtering and post-annealing for solar cells. *Ceram. Int.* **2019**, *45*, 3044–3051. [CrossRef]
35. Fang, Z.B.; Yan, Z.J.; Tan, Y.S.; Liu, X.Q.; Wang, Y.Y. Influence of post-annealing treatment on the structure properties of ZnO films. *Appl. Surf. Sci.* **2005**, *241*, 303–308. [CrossRef]
36. Gao, X.Y.; Wang, S.Y.; Li, J.; Zheng, Y.X.; Zhang, R.J.; Zhou, P.; Chen, L.Y. Study of structure and optical properties of silver oxide films by ellipsometry, XRD and XPS methods. *Thin Solid Film.* **2004**, *455*, 438–442. [CrossRef]